Infiltration in a double-porosity medium: Experiments and comparison with a theoretical model

Jolanta Lewandowska

Laboratoire d'étude des Transferts en Hydrologie et Environnement (LTHE), UMR 5564, CNRS, UJF, INPG, IRD, Grenoble, France

Adam Szymkiewicz and Wioletta Gorczewska

Institute of Hydroengineering, Polish Academy of Science, Gdańsk, Poland

Michel Vauclin

Laboratoire d'étude des Transferts en Hydrologie et Environnement (LTHE), UMR 5564, CNRS, UJF, INPG, IRD, Grenoble, France

Received 20 July 2004; revised 18 November 2004; accepted 7 December 2004; published 18 February 2005.

[1] This paper presents experimental verification of the mathematical model of unsaturated flow in double-porosity soils developed by the asymptotic homogenization method. A series of one-dimensional infiltration experiments was carried out in a column filled with a double-porosity medium composed of a mixture of sand and sintered clayey spheres arranged in a periodic manner. The unsaturated hydraulic properties of each porous material were obtained from independent infiltration experiments by inverse analysis and some additional tests. They were used to calculate the effective parameters of the double-porosity medium, i.e., the effective hydraulic conductivity and the effective capillary capacity. The numerical solution of the macroscopic boundary value problem, consisting of a highly nonlinear integrodifferential equation, was obtained using the Fortran code DPOR_1D presented by *Lewandowska et al.* [2004]. The calculated time evolutions of both water infiltrating into and flowing out from the double-porosity medium were compared with the experimental results. A very reasonable qualitative and quantitative agreement between simulations and observations is obtained, showing the capacity of the model to capture the main features of the process.

Citation: Lewandowska, J., A. Szymkiewicz, W. Gorczewska, and M. Vauclin (2005), Infiltration in a double-porosity medium: Experiments and comparison with a theoretical model, *Water Resour. Res.*, *41*, W02022, doi:10.1029/2004WR003504.

1. Introduction

[2] The term double-porosity is used to describe porous formations composed of two distinct subdomains with very different hydraulic properties. The difference comes from the contrasting characteristic pore sizes. Such media are often encountered in nature (soils, rocks). Because of the contrast in hydraulic parameters local nonequilibrium arises during transient water flow, which may have a major impact on pollutant transport, for example. This important effect cannot be captured by standard single-porosity model [*Richards*, 1931].

[3] A number of different approaches to modeling the unsaturated water flow in such media have been proposed in the literature (see *Šimůnek et al.* [2003] for the state of the art). Very often the phenomenological models, based on the concept of two overlapping subdomains [*Barenblatt et al.*, 1960; *Warren and Root*, 1963], are used. In that approach, one of the domains corresponds to a highly conductive system of fractures, macropores or interaggregate pores, while the other domain is associated with less permeable aggregates or porous blocks. The resulting model consists of two equations coupled by an exchange term, representing the water transfer between the two domains. This concept was used in the model proposed by *Gerke and van Genuchten* [1993a, 1993b], where flow within each subdomain is described by the Richards equation. The exchange term is assumed to be proportional to the difference in pressure heads between two subdomains through some geometry-dependent parameters and the conductivity of the interface [*Gerke and van Genuchten*, 1996]. Other propositions for the exchange term are also available [*Zimmerman et al.*, 1993; 1996; *Dykhuizen*, 1990; *Zimmerman and Bodvarsson*, 1989; *Barker*, 1985]. The modified version of the two-equation model, in which the second equation is reduced to the kinetic part is called the dual-porosity model [e.g., *Šimůnek et al.*, 2003].

[4] For macroporous or fractured soils different types of models were proposed by *Chen and Wagenet* [1992] and *Jarvis* [1994]. In the MACRO model of *Jarvis* [1994] the flow in the more conductive subdomain is described by the kinematic wave equation [*Germann and Beven*, 1985] and the water transfer from macropores to porous matrix is assumed to be proportional to the difference in saturations.

0043-1397/05/2004WR003504

[5] The nonequilibrium water flow in double-porosity media has been also studied using upscaling methods, where the macroscopic model is found from the microscopic description as a result of rigorous averaging procedures [*Arbogast et al.*, 1990; *Hornung*, 1991; *Quintard and Whitaker*, 1995; *Douglas et al.*, 1997]. A model of transient flow in unsaturated double-porosity soils has been recently presented by *Lewandowska et al.* [2004]. In that paper the homogenization method based on the asymptotic expansion technique was applied. It allows the derivation of a model which is intrinsic to the material and does not depend on the macroscopic boundary conditions. No assumption about the mathematical form of the model is needed. The local capillary and gravity driven flow within each domain is described by the Richards equation. The connectivity of the more conductive domain is a necessary condition. The other medium can be connected or forms inclusions. The resulting macroscopic model is a single integrodifferential equation with a nonlinear source term and two nonlinear effective parameters i.e., the effective hydraulic conductivity tensor and the effective capillary capacity. The effective hydraulic conductivity tensor can be calculated from the solution of the given local linear boundary value problem over the period, if the local geometry and the hydraulic conductivity of the more conductive domain are known. The domain of validity of the model is defined in terms of the capillary diffusivity ratio of the two subdomains and it is expressed as a power of the small parameter ε (scale separation parameter). Numerical simulations of two problems presented by *Lewandowska et al.* [2004] showed that this model gives results closer to the fine-scale reference solution than those obtained by the two-equation model of *Gerke and van Genuchten* [1993a, 1993b].

[6] Although modeling of flow in unsaturated double-porosity media has received much attention in the literature, the practical application of theoretical models is still somewhat limited. The main reason is that they require many parameters to be identified. In most practical cases those parameters cannot be directly measured and questions arise about the methods of their identification [see *Clothier et al.*, 1995; *Jaynes et al.*, 1995; *Schwartz et al.*, 2000; *Kätterer et al.*, 2001; *Köhne et al.*, 2002a, 2002b; *Logsdon*, 2002]. When the macroscopic parameters are identified by inverse techniques the verification of the model can be difficult, since in the analysis of the results one cannot distinguish between errors coming from different sources, like model errors, parameter errors, etc. [*Larsson and Jarvis*, 1999].

[7] The experimental verification of the *Gerke and van Genuchten* [1993a, 1993b] model was presented by *Šimůnek et al.* [2001]. A series of upward infiltration experiments were performed on undisturbed soil samples. The experimental results were analyzed using three different models: single-porosity equilibrium model, dual-porosity model and dual-permeability model. In each case the effective parameters of the macroscopic model were identified by the inverse technique. It was found that the nonequilibrium behavior can be well reproduced by both dual-porosity and dual-permeability models, which raises questions about the domain of validity of these models. *Gerke and Köhne* [2004] applied the model of *Gerke and van Genuchten* [1993a] to simulate bromide transport in a tile-drained agricultural field. The hydraulic parameters of the model were obtained from standard soil hydraulic measurements by adopting a bimodal fitting procedure. The transport parameters were inferred from soil column tracer experiments and geometrical transfer term parameters were empirically estimated from the soil structure description. The hydraulic conductivity and the diffusion coefficient appearing in the water and solute exchange terms were fitted by a calibration technique. A good agreement between numerical simulation and observations was obtained when the values of those two coefficients were significantly reduced as compared to the parameters of the weakly conductive soil matrix.

[8] The MACRO model of *Jarvis* [1994] was applied to a number of lysimeter experiments [*Saxena et al.*, 1994] or field-scale experiments [*Jarvis*, 1998; *Villholt et al.*, 1998; *Villholt and Jensen*, 1998; *Larsson and Jarvis*, 1999; *Ludwig et al.*, 1999]. In most cases the parameters of the model were obtained partially from independent measurements and partially by calibration. *Larsson and Jarvis* [1999] suggested the simplified description of interaction between the two subdomains and the uncertainty of boundary conditions as possible sources of discrepancy between simulations and observations. *Villholt and Jensen* [1998] calibrated their model by using different estimations of mass transfer parameters for early and later times of the process, in the latter case excessively small values were required to keep low exchange rate. The difficulty in estimating the parameters of the exchange term was also reported by *Ludwig et al.* [1999].

[9] This paper is aimed at presenting the experimental verification of the theoretical model developed by *Lewandowska et al.* [2004]. For that purpose, we considered a double-porosity medium, consisting of a mixture of fine sand and sintered clayey spheres arranged in a periodic manner. The hydraulic characteristics of each material were obtained from independent infiltration tests by inverse modeling. They were used to calculate the effective parameters of the double-porosity model by solving the local boundary value problem. Then, the macroscopic boundary value problem was solved using the effective parameters. The results of numerical simulations were compared with experimental data. The experiments with the double-porosity medium dealt with infiltration under constant pressure head into initially dry medium. The same kind of tests was performed in each material separately in order to keep similar initial and boundary conditions, and to avoid the possible influence of hysteresis.

[10] In the following sections are successively presented: (1) the theoretical model; (2) the infiltration experiments performed in sand, sintered clayey material and double-porosity medium, (3) the identification of the hydraulic parameters for each of the two constituting materials by inverse modeling, (4) the calculation of the effective parameters of the double-porosity medium, (5) the solution of the macroscopic boundary value problem, and (6) the comparison between the experimental and numerical results.

2. Modeling

[11] In this section we briefly describe the macroscopic model of water flow in double-porosity media obtained by the application of the homogenization technique [*Sanchez-*

Palencia, 1980; *Bensoussan et al.*, 1978; *Auriault*, 1991]. For more details, the reader is referred to the work of *Lewandowska et al.* [2004].

2.1. Assumptions

[12] The model was developed with the following assumptions: (1) the rigid porous medium has a periodic structure, the period (equivalent to the REV) being denoted by Ω, (2) the medium is composed of two porous subdomains: a more conductive connected matrix Ω_1 and less conductive inclusions Ω_2, with an interface Γ between them, (3) a separation of scales exists, which implies that $\varepsilon = l/L \ll 1$, where ε is a scale separation parameter, l is the size of the period and L is the size of the macroscopic domain, (4) the water flow is driven by capillary and gravity forces, (5) the air phase is assumed to be at the atmospheric pressure [*Richards*, 1931; *Bear*, 1972]; (6) the capillary effect dominates over the gravity effect at the local scale, (7) the ratio of the capillary diffusivities of the two subdomains is of the order $D_{2C}/D_{1C} = O(\varepsilon^2)$, (8) the characteristic time (the observation time) corresponds to the time of flow in the most conductive region at the macroscopic scale, and (9) the volumetric fractions of the two subdomains are of the same order, $O(w_1) = O(w_2)$.

2.2. Macroscopic Model

[13] According to *Lewandowska et al.* [2004], the macroscopic flow can be described by the following single integrodifferential nonlinear equation:

$$C^{eff}\frac{\partial h}{\partial t} - \frac{\partial}{\partial X_i}\left[K_{ij}^{eff}\left(\frac{\partial h}{\partial X_j} + I_{j3}\right)\right] + \frac{1}{|\Omega|}\int_{\Omega_2} C_2\frac{\partial h_2}{\partial t}\,\mathrm{d}\Omega = 0 \quad (1)$$

where h [L] is the macroscopic water pressure head which is a function of the volumetric water content θ (dimensionless), $C^{eff}(h)$ [L^{-1}] is the effective capillary capacity, $\mathbf{K}^{eff}(h)$ [LT^{-1}] is the effective hydraulic conductivity tensor, h_2 [L] and C_2 (h_2) [L^{-1}] are the local pressure head and the corresponding capillary capacity in the inclusions Ω_2, respectively, $\mathbf{X}$ [L] is the spatial coordinate (the X_3 axis being oriented positively upward) and t [T] is time.

[14] The integral term in equation (1):

$$Q = \frac{1}{|\Omega|}\int_{\Omega_2} C_2\frac{\partial h_2}{\partial t}\,\mathrm{d}\Omega \quad (2)$$

represents the nonequilibrium water exchange between the matrix subdomain Ω_1 and the inclusions Ω_2. It can be calculated by solving the additional local flow equation within the inclusion at each point of the macroscopic domain:

$$C_2\frac{\partial h_2}{\partial t} - \frac{\partial}{\partial Y_i}\left(K_2\frac{\partial h_2}{\partial Y_i}\right) = 0 \qquad i,j = 1,2,3 \quad \text{in } \Omega_2 \quad (3a)$$

with the pressure continuity condition at the interface Γ:

$$h_2 = h \qquad \text{on } \Gamma \quad (3b)$$

In equation (3a), $\mathbf{Y}$ [L] is the local spatial coordinate associated with a single period and $K_2(h_2)$ [LT^{-1}] is the local hydraulic conductivity of the inclusions (assuming that the material is isotropic). Note that gravity does not appear in equation (3a). This is a result of the estimation of the orders of magnitude and the homogenization procedure [*Lewandowska et al.*, 2004]. It should be noticed that the governing equation (1) obtained by homogenization fits into the traditional framework of dual-porosity models [e.g., *Zimmerman et al.*, 1996].

2.3. Effective Parameters

[15] If we assume that both subdomains are locally homogeneous and isotropic, then the effective parameters are defined as follows [*Lewandowska et al.*, 2004]:

$$C^{eff}(h) = w_1 C_1(h) \quad (4)$$

$$K_{ij}^{eff}(h) = K_1(h)\frac{1}{|\Omega|}\int_{\Omega_1}\left(\frac{\partial \chi_j}{\partial Y_i} + I_{ij}\right)\mathrm{d}\Omega \qquad i,j = 1,2,3 \quad (5)$$

where K_1 is the local hydraulic conductivity of the most conductive subdomain Ω_1 and the vector function χ is obtained from the solution of the following local boundary value problem in a single period:

$$\frac{\partial}{\partial Y_i}\left[\left(I_{ij} + \frac{\partial \chi_j}{\partial Y_i}\right)\right] = 0 \qquad i,j = 1,2,3 \qquad \text{in } \Omega_1 \quad (6)$$

$$\left(I_{ij} + \frac{\partial \chi_j}{\partial Y_i}\right)N_i = 0 \qquad i,j = 1,2,3 \qquad \text{on } \Gamma \quad (7)$$

χ is Ω periodic and

$$\int_{\Omega_2} \chi\,\mathrm{d}\Omega = 0 \quad (8)$$

where $\mathbf{N}$ is the unit vector normal to Γ. The function χ represents the influence of the local geometry on the macroscopic water transfer properties.

3. Experiments

3.1. Material

[16] The double-porosity medium used in the experiments was a mixture of Hostun sand HN38 [*Flavigny et al.*, 1990] and spheres made of sintered clayey material. The chemical composition of the sand is mainly quartz. The grain distribution is relatively uniform, with 51.2% of particles between 100 μm and 200 μm, the mean grain diameter being 162 μm. A series of laboratory standard compaction tests (see Polish soil standard PN-88/B-04481 Grunty budowlane: Analiza próbek gruntu) performed in a cylinder (12.6 cm high and 7.1 cm in diameter) gave porosity values ranging from $\phi_{min} = 0.412$ to $\phi_{max} = 0.538$.

[17] The sintered clayey spheres were made by hand in a pottery workshop. The clay originated from La Bisbal, Spain. It was washed and then fired at a temperature of 1000°C. The analysis by scanning electronic microscope showed that the clay material was relatively homogeneous, with no skin effect of reduced porosity close to the surface of the spheres. A mercury porosimetry test gave the porosity

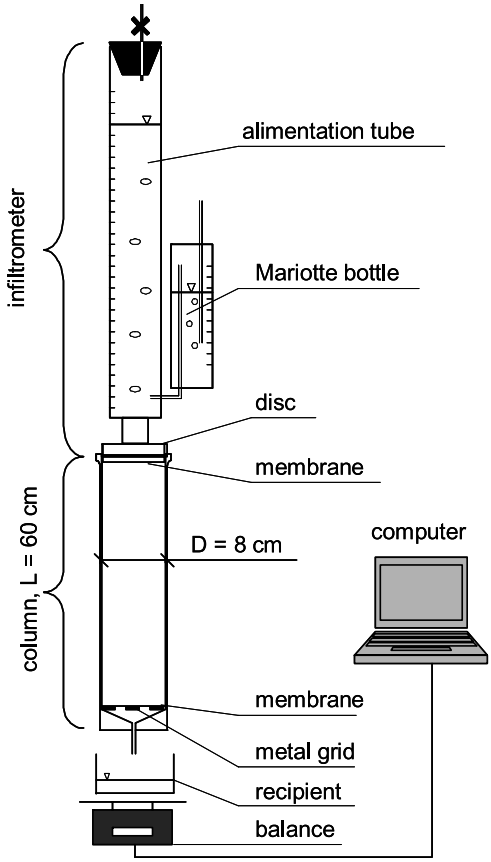

Figure 1. Experimental setup.

ϕ = 0.376 and the mean pore size around 0.7 μm. The skeleton specific density was ρ_s = 3.01 g/cm^3 and the dry bulk density ρ_d = 1.88 g/cm^3. The spheres were of relatively uniform diameter with an average value of 2R = 6.4 mm. Small numbers of spheres of diameter as small as 4.3 mm and as large as 9.4 mm were observed.

[18] Assuming that the characteristic size of the sand pores was of the same order of magnitude as the size of the grains, the contrast between pore sizes of both materials is of the order 1:230. Therefore some double-porosity effects may be expected.

3.2. Experimental Setup

[19] Infiltration tests were performed in a 60 cm high by 8 cm inner diameter clear acrylic column (Figure 1), in which the porous material was placed layer by layer. In the case of double-porosity medium the procedure was as follows. First, one layer of spheres was put in place, and then sand was poured until the spheres were completely covered. Next, the layer was mechanically compacted using a fixed number of blows of a small hammer. A tension disc infiltrometer with a porous membrane made of nylon (pore size of 20 μ) was placed on the surface of the column. The disc diameter was equal to that of the column, ensuring one-dimensional vertical flow. The infiltrometer consisted of a supply tube and a Mariotte bottle allowed a constant value of pressure head to be applied at the surface. The amount of water infiltrating into the column as a function of time was manually monitored. The accuracy of the measurements was estimated at ±0.6 mm of water.

[20] The porous medium was supported by a metal grid covered with a porous membrane (the same as at the inlet to the column). The water was allowed to freely flow out through the membrane into a vessel placed on a balance connected via a data logger (Campbell Scientific Ltd CR 10X) to a computer which registered the outflow water mass during the experiments in the double-porosity medium. For the experiments conducted in sand, the outflow measurements were taken manually. The maximum error of observations was 1 g, which corresponds to an accuracy of ±0.2 mm of water. The room temperature varied between 23° and 24°C.

3.3. Experiments in Sand

[21] In order to obtain the hydraulic characteristics of the sand, two experiments (tests 1 and 2) were carried out using the setup described above. The column was filled up with air-dry sand one day before each infiltration test. The initial volumetric water content was smaller than 0.001. The sand was put into the column in layers of about 1 cm and each layer was compacted in order to obtain the same sand porosity as in the experiments carried out with the double-porosity medium. We obtained ϕ = 0.399 in test 1 and ϕ = 0.407 in test 2. The pressure head imposed by the infiltrometer at the inlet of the column was $h_0 = -0.1$ cm of water. The cumulative infiltration and discharge volumes of water were manually registered. The breakthrough time, corresponding to the appearance of the first water drops at the outlet of the column was 3000 s in test 1 and 2490 s in test 2. In each case the infiltration was continued until the outflow reached a steady state regime (within the precision of the observations) and then beyond that time, until the supply tube was empty. At the end of each experiment the final water content θ_f was calculated from the difference between cumulative water inflow and discharge (expressed in cm) divided by the length of the column. The obtained values (θ_f = 0.338 in test 1 and θ_f = 0.346 in test 2) were significantly smaller than the porosity. This indicates that either a fraction of pores was inaccessible for water or some quantity of air remained trapped in the sand column as has been commonly reported by several authors [e.g., *Touma and Vauclin*, 1986; *Šimůnek et al.*,

Table 1. Some Characteristics of the Experiments Performed in the Double-Porosity Medium

Variable	Test 4	Test 5	Test 6	Mean	Coefficient of Variation, %
Volumetric fraction of sand w_1, dimensionless	0.447	0.444	0.443	0.445	0.47
Volumetric fraction of spheres w_2, dimensionless	0.553	0.556	0.557	0.555	0.37
Sand porosity ϕ, dimensionless	0.410	0.401	0.405	0.405	1.23
Final water content θ_f, dimensionless	0.290	0.290	0.300	0.293	1.97
Breakthrough time, s	5460	6000	5970	5810	5.20

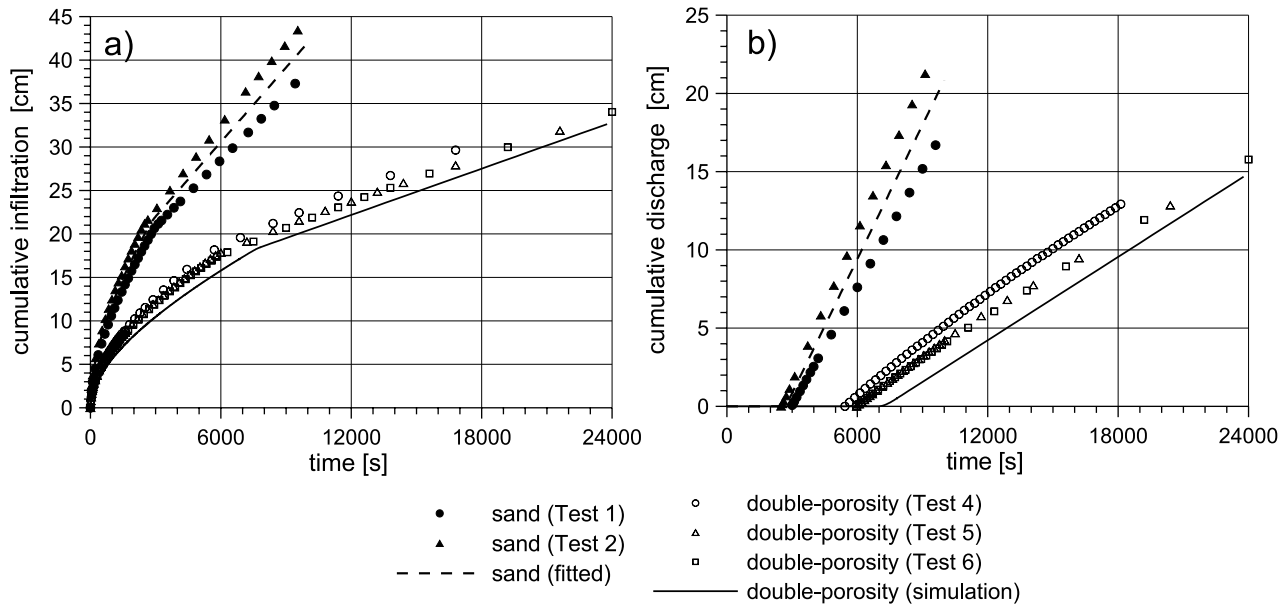

Figure 2. Measured and calculated values of (a) cumulative infiltration and (b) discharge in sand and double-porosity medium.

2001]. During the experiments the position of the wetting front was visually recorded.

3.4. Experiment in Sintered Clayey Material

[22] An infiltration experiment was carried out in a cylinder (25.9 cm high, 5.25 cm in diameter) made of the same material as the sintered clayey spheres (test 3). A small infiltrometer with a 5 cm diameter disc was placed on the top of the cylinder. Its lateral surface was isolated to avoid evaporation losses and by-pass flow. The material was air-dry and the initial volumetric water content was about 0.004. The applied water pressure head was $h_0 = -0.1$ cm. The volume of infiltrated water was manually registered. The experiment lasted about 60 h. After about 20 h we observed visible wetting of the bottom of the cylinder. No measurable amount of water flowing out of the cylinder was recorded.

3.5. Experiments in Double-Porosity Medium

[23] Three replications of the infiltration experiment were successively carried out in the double-porosity medium (tests 4, 5 and 6), using the setup described in section 3.2. One day before each test, the column was filled up with sand and spheres in a controlled manner, both porous media being initially air-dry. The spheres were put layer by layer in such a way that they were touching each other. From one layer to other the void space between spheres was carefully filled with sand, which was then compacted. By proceeding in this way a periodic arrangement was obtained. The volumetric fractions of spheres and sand, as well as the porosity of sand are given in Table 1. Small values of the coefficient of variation (CV) indicate a satisfying reproducibility of the way the column was filled up with the double-porosity medium. Consequently, the following mean values were retained for further analysis: volumetric fraction of sand $w_1 = 0.445$, volumetric fraction of spheres $w_2 = 0.555$ and porosity of sand $\phi = 0.405$.

[24] A pressure head of $h_0 = -0.1$ cm of water was imposed at the top of the column by means of the tension infiltrometer. The amount of water emanating from the disc was manually registered. The cumulative mass of water flowing out the base of the column was continuously monitored. The measured breakthrough times were: 5460 s, 6000 s and 5970 s for test 4, 5 and 6 respectively (Table 1). Each infiltration test lasted about 24 h and steady state flow regime was reached, at least within the precision of measurements. Final water contents varied between 0.29 and 0.3 with a mean of 0.293 and a CV of 1.97% (Table 1).

4. Hydraulic Characteristics of Sand and Sintered Clayey Material

4.1. Inverse Analysis

[25] It was assumed that both porous materials were adequately characterized by the van Genuchten–Mualem [*Mualem*, 1976; *van Genuchten*, 1980] closed-form relations:

$$\theta(h) = \theta_R + (\theta_S - \theta_R)[1 + (\alpha|h|)^n]^{-m} \tag{9}$$

$$K(h) = K_S\left[1 - (\alpha|h|)^{n-1}[1 + (\alpha|h|)^n]^{-m}\right]^2[1 + (\alpha|h|)^n]^{-m/2} \tag{10}$$

where θ_R and θ_S are the residual and saturated volumetric water content respectively, K_S is the saturated hydraulic conductivity [LT^{-1}], α [L^{-1}], n (dimensionless), and m (dimensionless) (with $m = 1 - 1/n$) are empirical constants. The total number of parameters to be determined is equal to 5 for each material.

[26] The HYDRUS_1D code [*Šimůnek et al.*, 1998] was used to identify by an inverse procedure the hydraulic parameters of sand and clayey material from the measured infiltration data. This was performed by minimizing the following objective function Φ expressed as

$$\Phi(\mathbf{b}) = \sum_{i=1}^{N}\left(I_{in}^{*} - I_{in}(\mathbf{b})\right)^2 + \sum_{j=1}^{M}\left(I_{out}^{*} - I_{out}(\mathbf{b})\right)^2 \tag{11}$$

Table 2. Parameters of the van Genuchten-Mualem Model for Sand and Sintered Clayey Material[a]

Parameter	Sand			Clayey Material (Test 3)
	Test 1	Test 2	Average	
θ_R, dimensionless	0.0	0.0	0.0	0.0
θ_S, dimensionless	0.338	0.346	0.342	0.295
α, cm^{-1}	**1.42×10^{-2}**	**1.34×10^{-2}**	1.38×10^{-2}	**6.05×10^{-3}**
n, dimensionless	**4.43**	**3.68**	4.06	**2.27**
K_S, cm s^{-1}	2.52×10^{-3}	3.20×10^{-3}	2.86×10^{-3}	**1.15×10^{-5}**

[a]Optimized values are shown in bold.

where **b** denotes the optimized parameter vector, I_{in}^* and I_{out}^* [L] are the measured cumulative infiltration and discharge amounts of water respectively, and I_{in}(**b**) and I_{out}(**b**) are the corresponding simulated values for a given set of parameters. N and M are the numbers of infiltration and discharge measurements, respectively. No weighting of the input data was considered and the Marquardt-Levenberg [*Marquardt*, 1963] algorithm was used for the minimization of Φ.

4.2. Sand

4.2.1. Conditions

[27] For tests 1 and 2 the measured cumulative infiltration and discharge values as function of time are presented in Figures 2a and 2b, respectively. The number of optimized parameters was two, namely α and n, the remaining three (θ_R, θ_S and K_S) having been estimated from additional considerations briefly explained below.

[28] We considered that $\theta_R = 0$. This can be justified by the fact that it should be less than the initial water content θ_n, which was measured in the initially air-dry conditions to be very small, $\theta_n < 0.001$.

[29] The volumetric water content at saturation θ_S was assumed to be equal to its final value as measured at the end of each test which is less than the porosity (Table 2).

[30] The hydraulic conductivity at saturation K_S was determined from an independent falling head test carried out in completely saturated conditions. The resulting value $K_S = 2.76 \times 10^{-3}$ cm/s was found to be close to the slopes of the cumulative inflow and discharge curves, measured when the steady state was attained. Consequently, in the inverse procedure, K_S was set to be equal to the value of these slopes, measured in each test (Table 2).

[31] The HYDRUS_1D code was run with the following boundary conditions: $h_0 = -0.1$ cm of water at the inlet and gravity drainage ($\partial h/\partial X_3 = 0$) at the outlet of the column. The initial condition was arbitrarily prescribed as $h_n = -1000$ cm of water. After fitting we obtained an initial value of the volumetric water content smaller than 0.001, which corresponds to the experimental conditions.

4.2.2. Results

[32] The inverse modeling approach was applied to tests 1 and 2 separately. The corresponding contour lines of the objective function Φ as a function of the fitted parameters α and n are presented in Figure 3. It can be seen that the surface of Φ shows a complex pattern with no well-defined global minimum. This makes the uniqueness of the solution questionable. Therefore the inverse procedure was repeated for several different initial values of the searched parameters. In each run, either the same minima were obtained or the solution was found to be unstable. Consequently, the values of α and n given in Table 2 for both tests were considered as the best estimates of the van Genuchten–Mualem parameters. They seem to be physically reasonable, in comparison with data reported in the literature for fine sand (R. Haverkamp et al., GRIZZLY, Grenoble Soil Catalogue: Survey of soil field data and description of particle size, soil water retention and hydraulic conductivity functions, Laboratoire d'étude des Transferts en Hydrologie et Environnement, Grenoble,

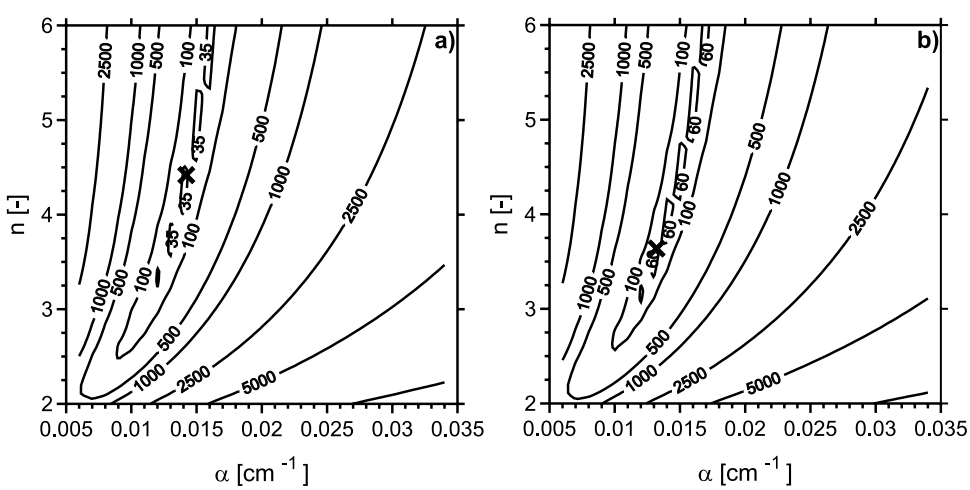

Figure 3. Contour lines of the objective function Φ (in cm^2) for sand in (a) test 1 and (b) test 2. The minimum is indicated by a marker.

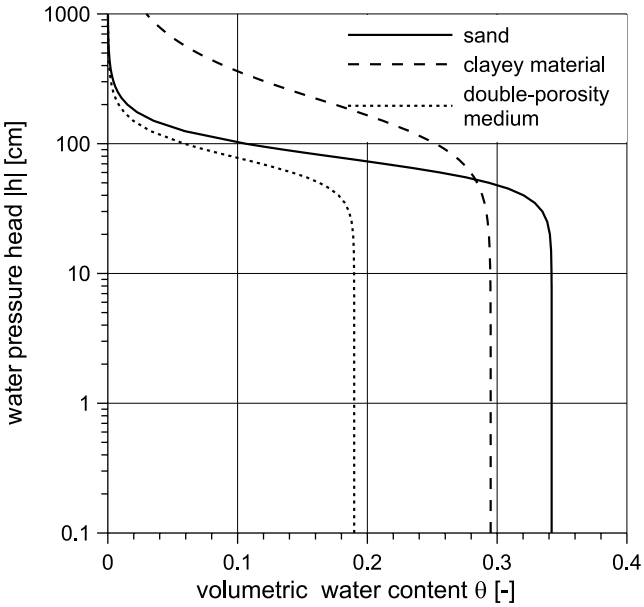

Figure 4. Retention curves of sand, sintered clayey material, and double-porosity medium.

France, 1998) (herinafter referred to as Haverkamp et al., Grenoble Soil Catalogue, 1998). In the following, their arithmetic means reported in Table 2 were retained. The resulting fitted cumulative infiltration and discharge amounts as function of time are drawn in Figure 2. The corresponding water retention and hydraulic conductivity curves calculated by equations (9) and (10) are plotted in Figures 4 and 5, respectively.

4.3. Sintered Clayey Material

4.3.1. Conditions

[33] In the inverse procedure the cumulative infiltration curve measured in test 3 (Figure 6) was used. Three

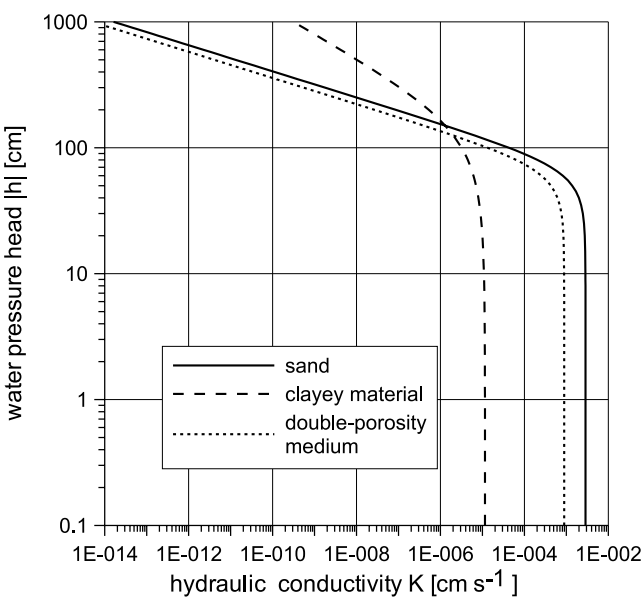

Figure 5. Hydraulic conductivity curves of sand, sintered clayey material, and double-porosity medium.

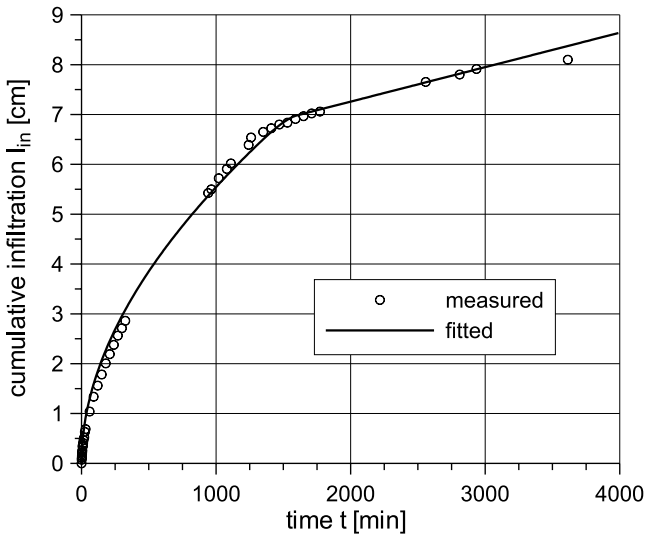

Figure 6. Measured and fitted time evolution of the cumulative infiltration in the sintered clayey material (test 3).

parameters were optimized: α, n and K_S. The residual water content was set at $\theta_R = 0$. The θ_S value was obtained from a series of additional saturation experiments (8 experiments). These consist of putting the porous spheres into free water and keeping them submerged until saturation was reached. The final volumetric water content varied from 0.283 to 0.30, with a mean of $\theta_f = 0.295$. Note that this value is significantly less than the porosity obtained by the mercury porosimetry test ($\phi = 0.376$). We assumed that θ_f corresponds to the fraction of pores effectively accessible to water during infiltration and consequently θ_S was set at $\theta_f = 0.295$ (Table 2).

[34] According to the experimental conditions, the boundary values used in the inverse modeling were: $h_0 = -0.1$ cm at the surface and free drainage ($\partial h/\partial X_3 = 0$) at the bottom of the cylinder ($X_3 = -25.9$ cm). The imposed initial condition was the same as for the sand ($h_n = -1000$ cm of water) since the hydraulic parameters of both materials were used in the double-porosity model which assumes initial equilibrium of pressure between the two subdomains.

4.3.2. Results

[35] The objective function Φ shows a well defined unique minimum (Figure 7). The corresponding parameters are given in Table 2 and the resulting fitted time evolution of cumulative infiltration is plotted in Figure 6. Not surprisingly, the parameter values appear different from those reported in the literature for clays (Haverkamp et al., Grenoble Soil Catalogue, 1998). As a matter of fact, it can be expected that the thermal treatment of clay caused some physical and chemical transformations of the material which have certainly influenced its hydraulic behavior. For example, the saturated hydraulic conductivity is of the same order of magnitude as the values reported for bricks [e.g., *Hall and Hoff*, 2003]. Also, it is worthwhile to note that the optimized saturated hydraulic conductivity (Table 2) is very close to the slope of the cumulative discharge measured during the steady state, $K_S = 1.11 \times 10^{-5}$ cm/s. The resulting water retention and hydraulic conductivity curves are reported

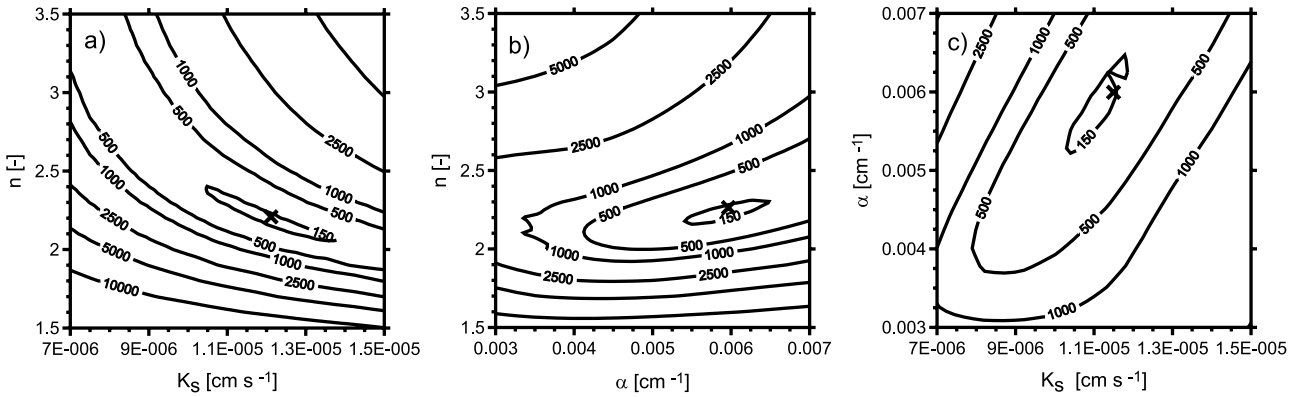

Figure 7. Contour lines of the objective function Φ (in mm^2) for the clayey material. The minimum is indicated by a marker.

in Figures 4 and 5, respectively. Note that the initial water content θ_n corresponding to $h_n = -1000$ cm of water is about 0.02, which is slightly higher than the measured value ($\theta_n = 0.004$).

5. Numerical Simulation of the Infiltration Into the Double-Porosity Medium

[36] The numerical simulation of the infiltration experiments was performed according to the mathematical model presented in section 2 which reads for 1D vertical flow as:

$$C^{eff}\frac{\partial h}{\partial t} - \frac{\partial}{\partial X_3}\left[K_{33}^{eff}\left(\frac{\partial h}{\partial X_3}+1\right)\right] + \frac{1}{|\Omega|}\int_{\Omega_2} C_2\frac{\partial h_2}{\partial t}\mathrm{d}\Omega = 0 \quad (12)$$

The calculations were carried out using the DPOR_1D Fortran code which was presented in *Lewandowska et al.* [2004] to simulate unsaturated water flow in a macroscopically one-dimensional domain with two- or three-dimensional inclusions.

[37] The calculations were made in two steps: (1) determination of the effective parameters and (2) solution of the macroscopic boundary value problem.

5.1. Periodic Double-Porosity Medium

[38] The double-porosity medium is considered as a periodic arrangement of spheres embedded in sand and touching each other. For this type of geometry, the volumetric fraction of spheres (w_2) can vary between 0.524 and 0.740, according to the distance between the successive layers. In our model, the geometry of the period was assumed to correspond to a volumetric fraction equal to $w_2 = 0.555$. This corresponds to the average value of the volumetric fraction of spheres measured in the three experiments (Table 1). The geometry of the period, which was used for the solution of the local boundary value problem and the determination of the effective conductivity, is shown in Figure 8. The dimensions of the period are 6.4 mm $\times$ 6.4 mm $\times$ 12.08 mm.

5.2. Determination of the Effective Parameters

[39] Both materials were assumed to be locally homogeneous and isotropic. In order to calculate the effective conductivity tensor, the local boundary value problem (6)–(8) has to be solved for χ in the 3D Ω_1 domain shown in Figure 8. For symmetry reasons, the effective conductivity tensor becomes:

$$\mathbf{K}^{eff} = \begin{vmatrix} K_{11}^{eff} & 0 & 0 \\ 0 & K_{22}^{eff} & 0 \\ 0 & 0 & K_{33}^{eff} \end{vmatrix},$$

where $K_{11}^{eff} = K_{22}^{eff}$. Since the problem is macroscopically one-dimensional, K_{33}^{eff} (denoted K^{eff} in the following) is the only component which is required to solve the macroscopic equation. Therefore, according to equation (5), χ_3 is the only component concerned. The local boundary value problem (6)–(8) was solved using the FEMLAB code [*COMSOL Group*, 2002]. The subdomain Ω_1 was discretized into 6946 elements (2042 nodes). Figure 9 shows the obtained solution for χ_3. Note the periodicity of χ_3 in three directions and its antisymmetry with respect to the plane (Y_1, Y_2). Using the values of χ_3, the effective hydraulic conductivity K^{eff} was calculated from equation (5) as

$$K^{eff}(h) = 0.310 \times K_1(h) \quad (13)$$

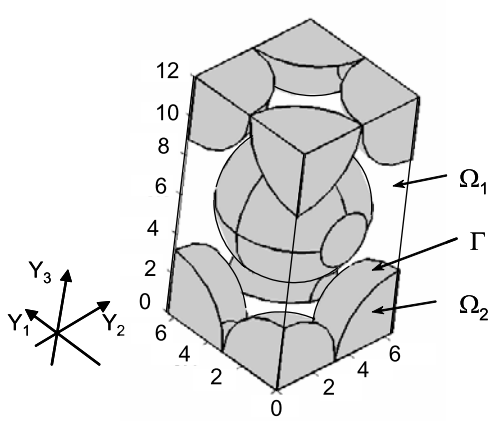

Figure 8. Period geometry. The subdomains Ω_1 (sand) and Ω_2 (sintered clayey sphere) are separated by the interface Γ. Units are in mm.

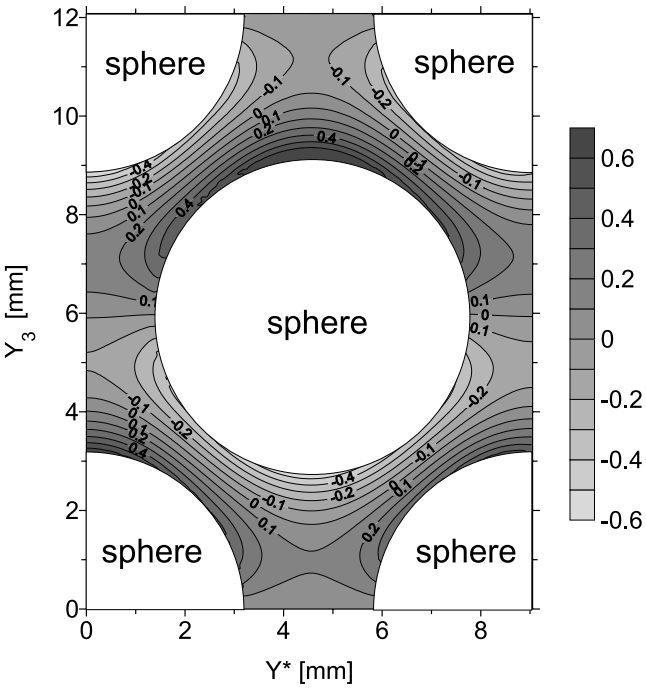

Figure 9. Solution of the local boundary problem, function χ_3. Cross section of the period along the diagonal plane ($Y_1 = Y_2$, Y_3).

The effective capillary capacity was calculated by equation (4) as

$$C^{eff}(h) = 0.445 \times C_1(h) \tag{14}$$

In equations (13) and (14), $K_1(h)$ and $C_1(h)$ are the hydraulic properties of the sand material. It should be noted that the coefficient 0.310 in equation (13) is different from the volumetric fraction of sand which is equal 0.445. The effective water retention and hydraulic conductivity curves of the double-porosity medium are reported in Figures 4 and 5, respectively. Note that the total water content present in a unit volume of the double-porosity medium cannot be calculated from the effective retention curve presented in Figure 5. This reflects the local non equilibrium present in the model.

5.3. Solution of the Macroscopic Flow Problem

5.3.1. Numerical Scheme

[40] The numerical algorithm implemented in the DPOR_1D code was used to solve equation (12). It is based on the mixed (θ-h) formulation suitable for the unsaturated flow equation [*Celia et al.*, 1990]. Consequently, equation (12) was discretized according to the following finite difference fully implicit scheme:

$$\frac{\theta_i^{j+1} - \theta_i^j}{\Delta t} - \frac{1}{\Delta X_3}\left[K_{i+1/2}^{j+1}\left(\frac{h_{i+1}^{j+1} - h_i^{j+1}}{\Delta X_3}\right) - K_{i-1/2}^{j+1}\left(\frac{h_i^{j+1} - h_{i-1}^{j+1}}{\Delta X_3}\right) + \left(K_{i+1/2}^{j+1} - K_{i-1/2}^{j+1}\right)\right] + Q_i^{j+1} = 0 \tag{15}$$

where i and j are space and time indices, respectively, θ (dimensionless) is the macroscopic volumetric water content corresponding to a given macroscopic pressure head h, ΔX_3 [L] is the space step, and Δt [T] is the time step. $K_{i\pm1/2}$ are the internodal effective hydraulic conductivities which were approximated by the arithmetic mean: $K_{i\pm1/2} = 0.5\,(K_i + K_{i\pm1})$ and Q [T^{-1}] is the integral sink term given by equation (2). Since θ, K and Q are highly nonlinear functions of h, the system was solved by the Newton method. The values of Q were obtained by solving the problem (3a)–(3b), which describes the local-scale flow in spheres. Each node (i, j) of the macroscopic one-dimensional grid is associated with a representative sphere, for which equation (3a) was solved. Taking into account the geometry of the inclusions, equation (3a) was rewritten in spherical coordinates, which results in the following equation:

$$\frac{\partial \theta_2(h_2)}{\partial t} - \frac{\partial}{\partial r}\left(K_2(h_2)\frac{\partial h_2}{\partial r}\right) - \frac{2}{r}\left(K_2(h_2)\frac{\partial h_2}{\partial r}\right) = 0 \tag{16}$$

where r is the radial coordinate ($0 < r < R = 0.32$ cm). The boundary conditions are: $h_2 = h$ at $r = R$ and $\partial h_2/\partial r = 0$ at $r = 0$. Equation (16) was discretized in a similar manner as equation (15) and the Picard method was used to solve the resulting nonlinear equations. The exchange term Q is then calculated from equation (2). The values of Q and its derivative dQ/dh which is required to solve equation (15) by the Newton method, were computed at each iteration. The time step was automatically adjusted according to the changes of h between two successive time levels.

[41] The parametric study of the spatial discretization (ΔX_3 in the range between 0.25 cm and 5 cm) showed a noticeable influence of ΔX_3 on the pressure profile for relatively large ΔX_3 (2.5 and 5 cm) but little influence on the inlet and outlet fluxes.

5.3.2. Macroscopic Boundary Value Problem

[42] The boundary conditions at the inlet and the outlet of the column were $h_0 = -0.1$ cm of water at $X_3 = 0$ and $\partial h/\partial X_3 = 0$ at $X_3 = -60$ cm. The initial

Table 3. Some Measured and Calculated Flow Characteristics Related to the Experiments Performed in the 60-cm-high Column Filled With Sand and Double-Porosity Medium

Variable	Sand Column		Double-Porosity Column	
	Measured[a]	Fitted	Measured[b]	Simulated
Breakthrough time, s	2750	2500	5810	7000
Volumetric flux at steady state regime, cm s^{-1}	2.86×10^{-3}	2.86×10^{-3}	8.46×10^{-4}	8.88×10^{-4}
Infiltrated water at breakthrough time, cm	21.1	20.0	17.7	17.3
Volumetric water content at steady state regime	0.342	0.342	0.293	0.316

[a]Mean values of tests 1 and 2.
[b]Mean values of tests 4, 5, and 6.

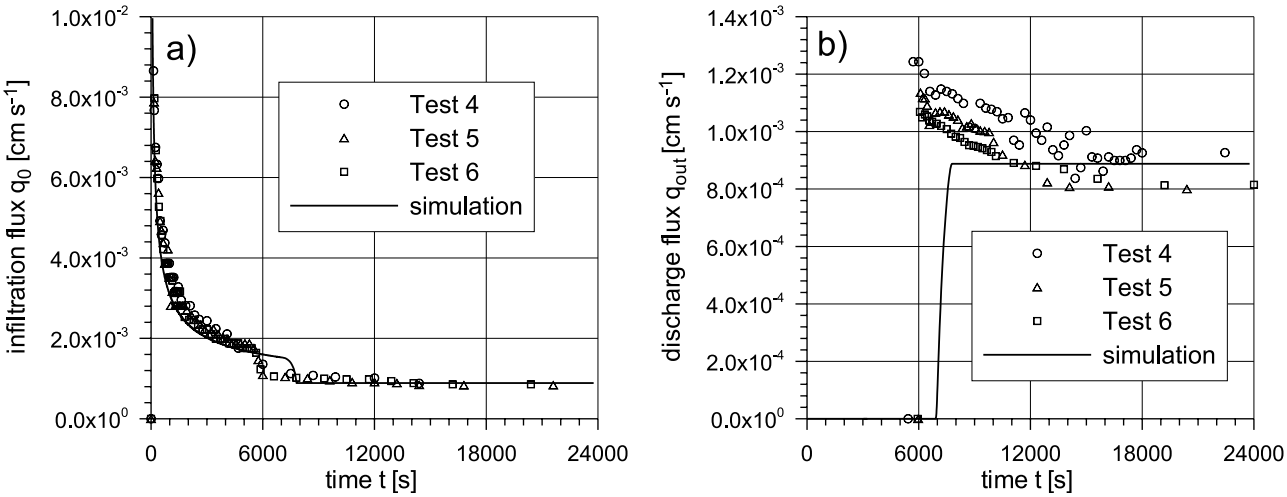

Figure 10. Comparison between measured and calculated (a) infiltration and (b) discharge fluxes in the double-porosity medium.

condition was imposed at $h_n = -1000$ cm within the whole domain, implying initial equilibrium between the two subdomains.

[43] The calculations were made with uniform space discretization of the macroscopic domain $\Delta X_3 = 0.5$ cm (121 nodes) as well as of the sphere domain $\Delta r = 0.016$ cm (21 nodes). The time step was allowed to vary from 10^{-6} s to 10 s. The accuracy was specified in terms of pressure head. A mixed criterion with an absolute tolerance of 0.1 cm of water and a relative tolerance of 0.1% was used. Finer grids ($\Delta X_3 = 0.25$ cm and $\Delta r = 0.0032$ cm) and smaller error tolerances were also tested but no significant influence on the results was observed.

6. Results and Discussion

6.1. Sand Versus Double-Porosity Medium Infiltration

[44] Table 3 gives some lumped parameters characterizing the infiltration both in sand and double-porosity medium. As can be seen, there are significant differences in all these parameters, whether they were measured or calculated. The observed breakthrough time in the double-porosity medium (5810 s) is about twice as long as in the sand (2750 s), while the factor is 2.8 for the calculated values. Both the measured and observed fluxes at quasi steady state regime (and almost saturation) are three times greater in sand than in double-porosity medium. The total measured amount of water infiltrated into the column is about 16% less in the case of the double-porosity medium than in sand. This result is confirmed by the numerical simulation. We also notice a difference between the mean final volumetric water content measured in sand (0.342) and in the double-porosity medium (0.293), which can be explained by the difference in porosities between sand and sintered clayey material. The final measured water content in the double-porosity medium (0.293) can be compared with its total porosity (0.316), calculated as the average of the porosity accessible to water in sand (0.342) and clayey material (0.295). The experimental value is slightly smaller, which indicates that the porous spheres were not completely saturated (in the reduced fraction of their porosity, assumed to be accessible to water).

6.2. Experimental Versus Simulated Water Flow in the Double-Porosity Medium

6.2.1. Infiltration and Discharge Curves

[45] The comparison between the observed and simulated behavior of the double-porosity medium is presented in Figures 2 and 10. The measured cumulative infiltration curves are well reproduced by the numerical solution (Figure 2). The measured and calculated instantaneous fluxes (Figure 10) seem to be in a reasonable agreement. However, in all three experiments the infiltration process occurred faster than obtained by the numerical simulation. Moreover, the measured early stage discharge flux (Figure 10b) is significantly greater than the water conductivity at steady state for $h = -0.1$ cm. This indicates the presence of a capillary pressure gradient at the bottom of the column. No such effect was observed in the tests with sand, which were performed in the same experimental conditions. Thus we believe that it can be associated to the air phase flow, i.e., air pressure can not equilibrate instantaneously, as is assumed in the model, and therefore it is not constant during the process. This effect should be further examined. The observed steady state fluxes in Figure 10, corresponding to the water conductivity at $h = -0.1$ cm, are very close to the calculated conductivity at saturation (Table 3). This confirms the validity of the method of calculation of the effective water conductivity obtained by homogenization, as a solution of the local boundary value problem (6)–(8). It also confirms our assumption, concerning the arrangement of clayey spheres (Figure 8).

6.2.2. Sensitivity Analysis of the Macroscopic Model

[46] In order to examine the sensitivity of the model with respect to the hydraulic parameters of both sand and clayey spheres, a series of numerical simulations were performed with different values of the parameters of the van Genuchten relations. In particular, the influence of the parameters α and n of both media was studied. It was

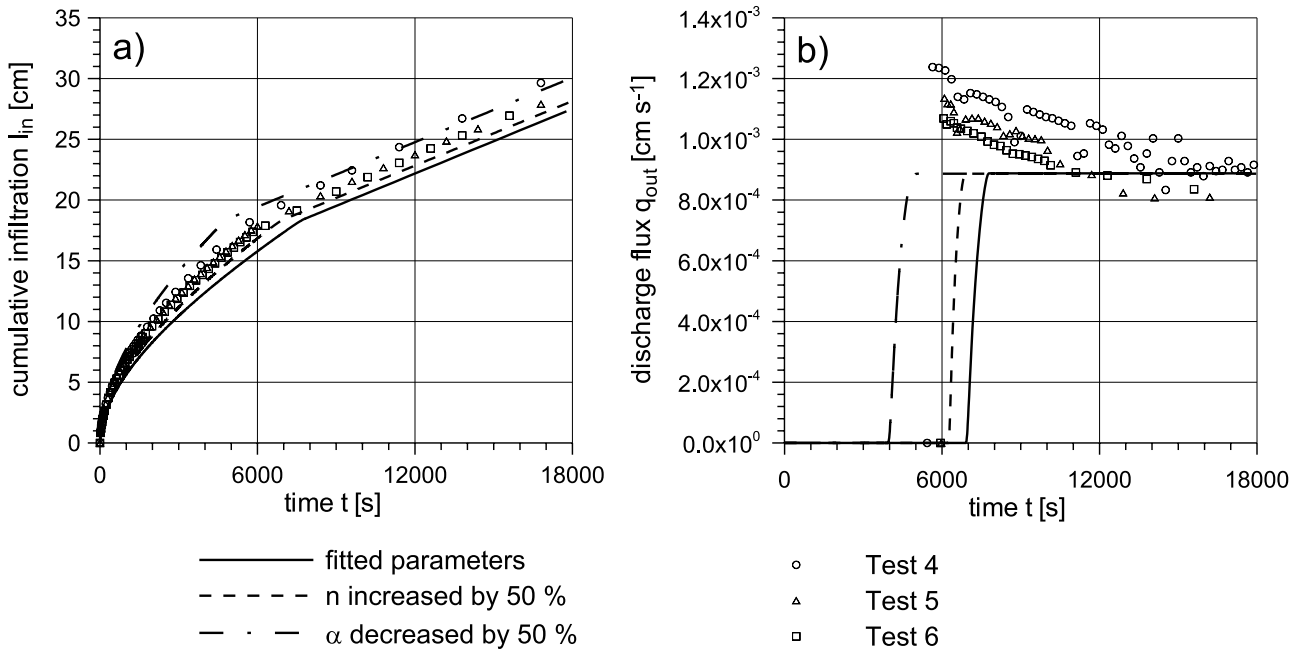

Figure 11. Influence of the sand parameters of the van Genuchten model on (a) the calculated cumulative infiltration and (b) the calculated discharge flux in the double-porosity medium.

found that the model was more sensitive to the parameters of sand than to the parameters of the clayey spheres. As an example, Figure 11 shows that better agreement can be obtained between calculated and observed values by increasing n for sand by 50% (or decreasing α by 50%). Nevertheless, no further attempt to obtain a better fit to the experimental data was carried out.

6.2.3. Exchange Term

[47] Figure 12 shows the values of the water exchange rate Q computed at selected depths in the column. It can be seen that the rate of the water exchange changes very rapidly with time, reaching high values at the arrival of the infiltration front and also diminishing rapidly. The characteristic time of the water transfer is relatively short as compared to the breakthrough time in the column. The maximum value of the exchange rate decreases with time while the duration of the exchange increases.

[48] In Figure 13 the calculated time evolutions of flux at the bottom of the column for the double-porosity medium and two other systems are compared. In the first case the spheres were assumed completely impermeable, while in the second case there are no inclusions. It can be seen that the presence of inclusions in the sand leads to the retardation of the flux. This effect increases very significantly when the inclusions are permeable, due to the exchange between the two pore systems. Moreover, with respect to

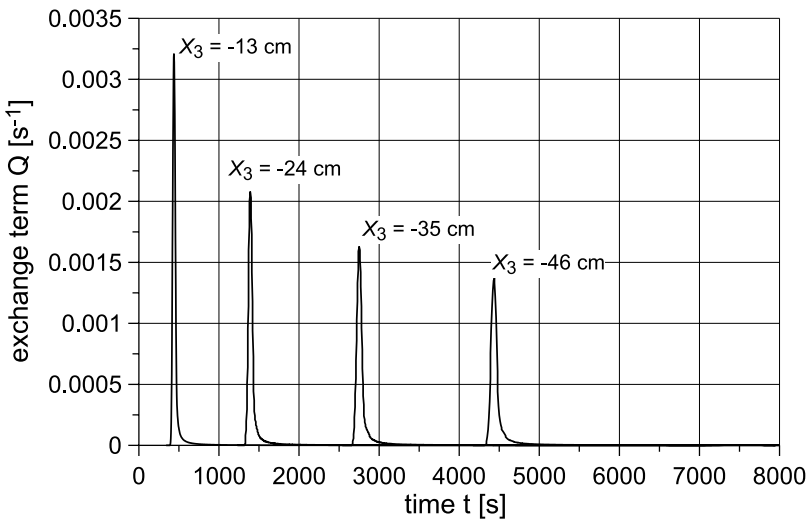

Figure 12. Time evolution of the water exchange term between sand and sintered clayey spheres calculated at different depths (X_3) of the column.

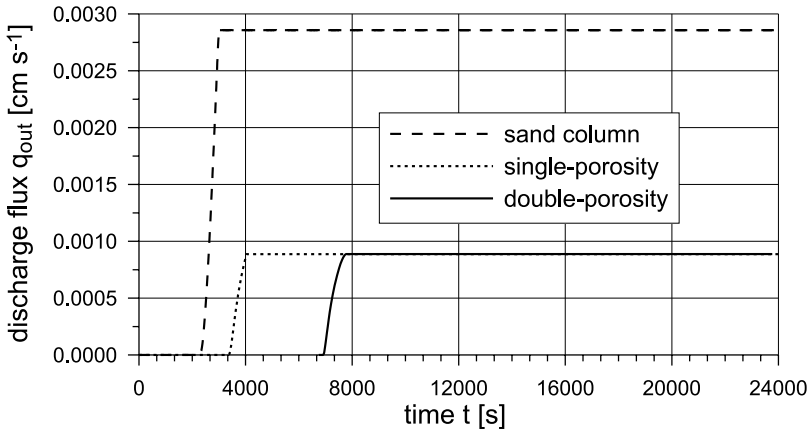

Figure 13. Comparison between the outflow fluxes calculated for the double-porosity medium, the single-porosity medium (impermeable spheres), and the sand column.

pure sand the permeable inclusions cause a significant decrease in the steady state flux.

6.3. Domain of Validity of the Double-Porosity Model

[49] It is reminded that the domain of validity of the model is defined by the ratio of the capillary diffusivities of the two media. It should be such that

$$D_{2C}/D_{1C} = \mathrm{O}(\varepsilon^2) \tag{17}$$

The parameter ε being equal to the ratio of the period size to the column length, ε = 1.2 cm/60 cm $\sim 10^{-2}$, so equation (17) leads to

$$D_{2C}/D_{1C} = \mathrm{O}(10^{-4}) \tag{18}$$

Figure 14 presents the ratio of the hydraulic properties of the two media as a function of water pressure head. It can be seen that D_{2C}/D_{1C} varies between 10^{-6} for $h = -0.1$ cm and 10^2 for $h = -1000$ cm. It means that the present model is not applicable during the whole infiltration process. It is only valid when h falls in the range between -1 cm ($D_{2C}/D_{1C} = \mathrm{O}(10^{-5})$) and -10 cm ($D_{2C}/D_{1C} = \mathrm{O}(\varepsilon^{-3})$. Outside this domain two other models are applicable (Figure 14), namely, either the equilibrium model for moderately heterogeneous medium [*Lewandowska and Laurent*, 2001] or the equilibrium model for soils containing inclusions more conductive than the matrix [*Lewandowska and Auriault*, 2003]. Finally, it should be concluded that in our experiment various effects were superposed and the double-porosity features are "hidden." Therefore another experiment is foreseen such that the condition $D_{2C}/D_{1C} = \mathrm{O}(\varepsilon^2)$ will be satisfied during the entire process of infiltration.

7. Conclusions

[50] In order to verify the double-porosity unsaturated flow model obtained from homogenization and the associated numerical model, infiltration experiments were carried out on mixtures of fine sand and sintered clayey spheres packed periodically in a column.

[51] The general conclusion is that the model seems to be able to correctly reproduce the main characteristic features which were observed. In particular, the saturated effective conductivity of the double-porosity medium calculated by the model is in a very good agreement with the observations. Nevertheless, it is difficult to conclude in a definite way, since the domain of validity of the double-porosity model did not completely fit the experimental conditions. Also, the validity of the van Genuchten-Mualem relation for describing the hydraulic properties of the two materials, as well as some assumptions underlying the Richards equation, would require a deeper analysis by performing more detailed experiments which are currently in progress.

[52] Despite some shortcomings and limitations of the present analysis we believe that this type of study is a valuable contribution to a better understanding of processes in complex unsaturated porous media.

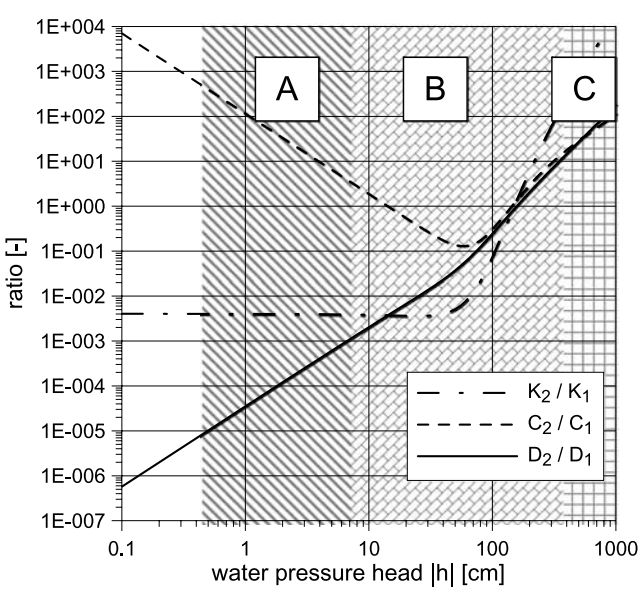

Figure 14. Domain of validity. Zone A is the double-porosity model. Zone B is the local equilibrium model [*Lewandowska and Laurent*, 2001]. Zone C is the local equilibrium model [*Lewandowska and Auriault*, 2003]. Subscript 1, sand; subscript 2, sintered clayey material.

Notation

b optimized parameter vector.
C_1, C_2 capillary capacity of medium 1 (sand) and 2 (clay) [L^{-1}].
C^{eff} effective capillary capacity of the double-porosity medium [L^{-1}].
CV coefficient of variation (dimensionless).
D capillary diffusivity [L^2 T^{-1}].
h_0 water pressure head imposed at the surface [L].
h_n initial water pressure head [L].
h_1, h_2 water pressure head in medium 1 and 2 [L].
I identity matrix.
I cumulative amount of water [L].
K hydraulic conductivity tensor [L T^{-1}].
K^{eff} effective hydraulic conductivity of the double-porosity medium [L T^{-1}].
K_S hydraulic conductivity at saturation [L T^{-1}].
L macroscopic domain size [L].
l characteristic period size [L].
m water retention function parameter (dimensionless).
N unit vector normal to the interface Γ.
n water retention function parameter (dimensionless).
Q water exchange rate between medium 1 and 2, [T^{-1}].
q_0 volumetric water flux at the surface [L T^{-1}].
q_{out} outflow flux [L T^{-1}].
R mean radius of sintered clayey sphere [L].
r radial coordinate [L].
t time [T].
w_1, w_2 volumetric fractions of medium 1 and 2 (dimensionless).
X macroscopic space coordinate [L].
Y local space coordinate [L].
α water retention function parameter [L^{-1}].
Γ interface between medium 1 and 2.
Δt time step [T].
ΔX_3 space step [L].
ε scale separation parameter (dimensionless).
ϕ porosity (dimensionless).
Φ objective function.
ρ_d bulk density [M L^{-3}].
ρ_s skeletal density [M L^{-3}].
θ volumetric water content (dimensionless).
θ_R residual volumetric water content (dimensionless).
θ_S saturated volumetric water content (dimensionless).
χ vector function, solution of the local boundary value problem (dimensionless).
Ω period domain.
Ω_1, Ω_2 domains of the period occupied by medium 1 and 2.

[53] **Acknowledgments.** The authors are grateful to their colleagues R. Angulo-Jaramillo, J. P. Gaudet and J. F. Daïan for fruitful discussions dealing with the experimental data analysis. J. M. Lapetite, M. Ricard and S. Boubkraoui are kindly acknowledged for their technical assistance in the preparation of the experiment. We thank J. J. Dubernard (Poterie des Chals in Roussillon, France) for manufacturing the clayey spheres. This research was funded by the French Project ECCO PNRH 2003 "Transferts complexes en milieux poreux et ressources en eau". The French Ministry of Foreign Affairs and the Région Rhône-Alpes (MIRA Program) are greatly acknowledged for the Ph.D. scholarship granted to A. Szymkiewicz. The research work of A. Szymkiewicz and W. Gorczewska was carried out in the framework of the collaboration agreement between the Laboratoire LTHE, Grenoble, France and Gdańsk University of Technology, Poland.

References

Arbogast, T., J. Douglas Jr., and U. Hornung (1990), Derivation of the double porosity model of single phase flow via homogenization theory, *SIAM J. Math. Anal.*, *21*, 823–836.

Auriault, J.-L. (1991), Heterogeneous medium: Is an equivalent macroscopic description possible?, *Int. J. Eng. Sci.*, *29*(7), 785–795.

Barenblatt, G. I., I. P. Zheltov, and I. N. Kochina (1960), Basic concepts in the theory of seepage of homogeneous liquids in fissured rocks, *J. Appl. Math.*, *24*(5), 1286–1303.

Barker, J. A. (1985), Block-geometry functions characterizing transport in densely fissured media, *J. Hydrol.*, *77*, 263–279.

Bear, J. (1972), *Dynamics of Fluids in Porous Media*, Elsevier, New York.

Bensoussan, A., J.-L. Lions, and G. Papanicolaou (1978), *Asymptotic Analysis for Periodic Structures*, Elsevier, New York.

Celia, M. A., E. T. Bouloutas, and R. L. Zarba (1990), A general mass-conservative numerical solution for the unsaturated flow equation, *Water Resour. Res.*, *26*(7), 1483–1496.

Chen, C., and R. J. Wagenet (1992), Simulation of water and chemicals in macropore soils. part 1: Representation of the equivalent macropore influence and its effect on soil water flow, *J. Hydrol.*, *130*, 105–126.

Clothier, B. E., L. Heng, G. N. Magesan, and I. Vogeler (1995), The measured mobile-water content of an unsaturated soil as a function of hydraulic regime, *Aust. J. Soil Res.*, *33*, 397–414.

COMSOL Group (2002), FEMLAB users manual, version 2.3.01.148, Burlington, Mass.

Douglas, J., M. Peszyńska, and R. Showalter (1997), Single phase flow in partially fissured media, *Transp. Porous Media*, *278*, 285–306.

Dykhuizen, R. C. (1990), A new coupling term for dual-porosity models, *Water Resour. Res.*, *26*(2), 351–356.

Flavigny, E., J. Desrues, and B. Palayer (1990), Le sable d'Hostun "RF": Note technique, *Rev. Fr. Geotech.*, *53*, 67–69.

Gerke, H. H., and J. M. Köhne (2004), Dual-permeability modeling of preferential bromide leaching from a tile-drained glacial till agricultural field, *J. Hydrol.*, *289*, 239–257.

Gerke, H. H., and M. T. van Genuchten (1993a), A dual-porosity model for simulating the preferential movement of water and solutes in structured porous media, *Water Resour. Res.*, *29*(2), 305–319.

Gerke, H. H., and M. T. van Genuchten (1993b), Evaluation of a first-order water transfer term for variably saturated dual-porosity flow models, *Water Resour. Res.*, *29*(4), 1225–1238.

Gerke, H. H., and M. T. van Genuchten (1996), Macroscopic representation of structural geometry for simulating water and solute movement in dual-porosity media, *Adv. Water Resour.*, *19*(6), 343–357.

Germann, P. F., and K. Beven (1985), Kinematic wave approximation to infiltration into soils with sorbing macropores, *Water Resour. Res.*, *21*(7), 990–996.

Hall, C., and W. D. Hoff (2003), *Transport in Brick, Stone and Concrete*, Taylor and Francis, Philadelphia, Pa.

Hornung, U. (1991), Homogenization of miscible displacement in unsaturated aggregated soils, in *Composite Media and Homogenization Theory*, *Prog. Nonlinear Differ. Equations Their Appl.*, vol. 5, edited by G. dal Maso and F. Dell'Antonio, pp. 143–153, Springer, New York.

Jarvis, N. J. (1994), The MACRO model ver. 3.1: Technical description and sample simulations, *Rep. Diss. 19*, 51 pp., Dep. of Soil Sci., Swed. Univ. of Agric. Sci., Uppsala.

Jarvis, N. J. (1998), Modeling the impact of preferential flow on nonpoint source pollution, in *Physical Nonequilibrium in Soils: Modeling and Application*, edited by H. M. Selim and L. Ma, pp. 195–221, CRC Press, Boca Raton, Fla.

Jaynes, D. B., S. D. Logsdon, and R. Horton (1995), Field method for measuring mobile/immobile water content and solute transfer rate coefficient, *Soil Sci. Soc. Am. J.*, *59*, 352–356.

Kätterer, T., B. Schmied, K. C. Abbaspour, and R. Schulin (2001), Single and dual-porosity modeling of multiple tracer transport through soil columns: Effects of initial moisture and mode of application, *Eur. J. Soil Sci.*, *52*, 25–36.

Köhne, J. M., H. H. Gerke, and S. Köhne (2002a), Effective diffusion coefficients of soil aggregates with surface skins, *Soil Sci. Soc. Am. J.*, *66*(5), 1430–1438.

Köhne, J. M., S. Köhne, and H. H. Gerke (2002b), Estimating the hydraulic functions of dual-permeability models from bulk soil data, *Water Resour. Res.*, *38*(7), 1121, doi:10.1029/2001WR000492.

Larsson, M. H., and N. J. Jarvis (1999), Evaluation of a dual-porosity model to predict field-scale solute transport in a macroporous soil, *J. Hydrol.*, *215*, 153–171.

Lewandowska, J., and J.-L. Auriault (2003), Modeling of unsaturated flow in soils with highly permeable inclusions, *C. R. Acad. Sci., Ser. IIB Mec.*, *332*, 91–96.

Lewandowska, J., and J.-P. Laurent (2001), Homogenization modeling and parametric study of moisture transfer in an unsaturated heterogeneous porous medium, *Transp. Porous Media*, *45*, 321–345.

Lewandowska, J., A. Szymkiewicz, K. Burzyński, and M. Vauclin (2004), Modeling of unsaturated water flow in double porosity soils by the homogenization approach, *Adv. Water Resour.*, *27*(3), 283–296.

Logsdon, S. D. (2002), Determination of preferential flow model parameters, *Soil Sci. Soc. Am. J.*, *66*, 1095–1103.

Ludwig, R., H. H. Gerke, and O. Wendroth (1999), Describing water flow in macroporous field soils using the modified macro model, *J. Hydrol.*, *215*, 135–152.

Marquardt, D. W. (1963), An algorithm for least-squares estimation of nonlinear parameters, *SIAM J. Appl. Math.*, *11*, 431–441.

Mualem, Y. (1976), A new model for predicting the hydraulic conductivity of unsaturated porous media, *Water Resour. Res.*, *12*(3), 513–522.

Quintard, M., and S. Whitaker (1995), Transport in chemically and mechanically heterogeneous porous media. I: Theoretical development of region averaged equations for slightly compressible single phase flow, *Adv. Water Resour.*, *19*(1), 29–47.

Richards, L. A. (1931), Capillary conduction of liquids through porous medium, *Physics*, *1*, 318–333.

Sanchez-Palencia, E. (1980), *Non-homogeneous Media and Vibration Theory*, *Lect. Note Phys.*, vol. 127, Springer, New York.

Saxena, R. K., N. J. Jarvis, and L. Bergström (1994), Interpreting non-steady state tracer breakthrough experiments in sand and clay soils using a dual porosity model, *J. Hydrol.*, *162*, 279–298.

Schwartz, R. C., A. S. R. Juo, and K. J. McInnes (2000), Estimating parameters for a dual-porosity model to describe non-equilibrium, reactive transport in a fine-textured soil, *J. Hydrol.*, *229*, 146–167.

Šimůnek, J., M. Šejna, and M. T. van Genuchten (1998), HYDRUS 1D software package for simulating the one-dimensional movement of water heat and multiple solutes in variably saturated media, version 2.0, Int. Ground Water Model. Cent., Colo. Sch. of Mines., Golden.

Šimůnek, J., O. Wendroth, N. Wypler, and M. T. van Genuchten (2001), Non-equilibrium water flow characterized by means of upward infiltration experiments, *Eur. J. Soil Sci.*, *52*, 13–24.

Šimůnek, J., N. J. Jarvis, M. T. van Genuchten, and A. Gärdenäs (2003), Review and comparison of models for describing non-equilibrium and preferential flow and transport in the vadose zone, *J. Hydrol.*, *272*, 14–35.

Touma, J., and M. Vauclin (1986), Experimental and numerical analysis of two phase infiltration in a partially saturated soil, *Transp. Porous Media*, *1*, 27–55.

van Genuchten, M. T. (1980), A closed form equation for predicting the hydraulic conductivity of unsaturated soils, *Soil Sci. Soc. Am. J.*, *44*, 892–898.

Villholt, K. G., and K. H. Jensen (1998), Flow and transport processes in a macroporous subsurface drained glacial till soil: II. Model analysis, *J. Hydrol.*, *207*, 121–135.

Villholt, K. G., K. H. Jensen, and J. Fredericia (1998), Flow and transport processes in a macroporous subsurface drained glacial till soil: I. Field investigations, *J. Hydrol.*, *207*, 98–120.

Warren, J. E., and P. J. Root (1963), The behaviour of naturally fractured reservoirs, *Soc. Pet. Eng. J.*, *3*, 245–255.

Zimmerman, R. W., and G. S. Bodvarsson (1989), Integral method solution for diffusion into a spherical block, *J. Hydrol.*, *111*, 213–224.

Zimmerman, R. W., G. Chen, T. Hadgu, and G. S. Bodvarsson (1993), A numerical dual-porosity model with semianalytical treatment of fracture/matrix flow, *Water Resour. Res.*, *29*(7), 2127–2137.

Zimmerman, R. W., T. Hadgu, and G. S. Bodvarsson (1996), A new lumped-parameter model for flow in unsaturated dual-porosity media, *Adv. Water Resour.*, *19*(5), 317–327.

W. Gorczewska and A. Szymkiewicz, Institute of Hydroengineering, Polish Academy of Science, ul. Kościerska 7, 80-953 Gdańsk, Poland.

J. Lewandowska and M. Vauclin, Laboratoire d'étude des Transferts en Hydrologie et Environnement (LTHE), UMR 5564, CNRS, UJF, INPG, IRD, BP53, 38041 Grenoble Cedex 09, France. (jolanta.lewandowska@hmg.inpg.fr)